



# Advanced Virgo Squeezer Technical Design Report

VIR-xxxA-12

*Issue 1*

Magari Mettiamo la lista

July 14, 2014



# Contents

<b>1</b>	<b>Chapter</b>	<b>1</b>
<b>2</b>	<b>Chapter</b>	<b>3</b>
<b>3</b>	<b>Chapter</b>	<b>5</b>
<b>4</b>	<b>Chapter</b>	<b>7</b>
<b>5</b>	<b>Homodyne detection</b>	<b>9</b>
5.1	Squeezing diagnostic homodyne detection . . . . .	9
5.1.1	The detection board . . . . .	9
5.1.2	The photodiode selection . . . . .	12
5.1.3	The readout blocks . . . . .	17
5.1.4	Noise budget . . . . .	23



**Chapter 1**

**Chapter**

**Introduction**



**Chapter 2**

**Chapter**

**Introduction**



## Chapter 3

# Chapter

### Introduction



**Chapter 4**

**Chapter**

**Introduction**



# Chapter 5

## Homodyne detection

### 5.1 Squeezing diagnostic homodyne detection

A phase dependent detection scheme is required in order to characterize squeezed light and the typical detection scheme used for that purpose is the balanced homodyne detection. A balanced homodyne detector consists of a 50/50 beam splitter where two optical fields  $\hat{a}$  and  $\hat{b}$  are superimposed. The resulting fields are detected by means of two photodiodes so that the sum and difference of the corresponding photocurrents are measured. One of the two fields is the squeezed field while the other one is a the local oscillator, i.e a strong coherent field, which we use as phase reference.

However, the balancing of both the optical and electronic components is crucial. Indeed, a non-perfect interference at the beam splitter results in an *optical unbalance*, that can be due to a beam mismatching, in term of spatial mode, wave front curvature, polarization and frequency, of the tow fields which mix at the beam splitter. The quality of the interference is characterized by the fringe visibility, and it can be used as parameter to determine the homodyne efficiency from the optical point of view. We have to consider also the *electronic unbalance* that can be caused by different quantum efficiencies and different electronic read-out gains of the two photodiodes used for the detection. Obviously both the possible unbalances degrade the capability of the homodyne detection of the squeezed light, so that the measured squeezing would be lower than the real one.

The degradation of the detected squeezing from the ideal case produced by both the above-mentioned unbalances is shown in fig. 5.1 and 5.2, plotting the difference between the real squeezing value ( $V_{real}$ ) and the measured one ( $V_{meas}$ ) as a function of the considered parameters (initial squeezing value, electronic gain and beam splitter reflectivity).

In this chapter we present an homodyne detector, mainly dealing with the issues concerning the electronic unbalance and noises. For the optical unbalancing issue see ??.

#### 5.1.1 The detection board

A conceptual scheme of the electronic board proposed for the homodyne detection is shown in fig. 5.3, where the main blocks of the electronic circuit are indicated. The most important features are:

- the *two photodiodes* are selected in order to have *identical characteristics*;

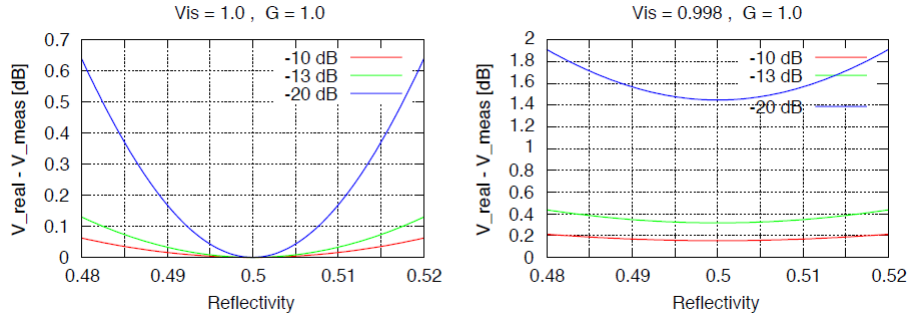


**Figure 5.1.** Beam splitter unbalance dependence of the squeezing detection efficiency. Taking the electronic gain to be  $G = 1$ , depending on the initial squeezing value ( $10dB$ ,  $13dB$  and  $20dB$ ) and varying the beam splitter reflectivity  $R$ , the measured squeezing ( $V_{meas}$ ) diminishes with respect to the real one ( $V_{real}$ ). The situation is even worse if we allow a non perfect fringe visibility (shown in the right panel).

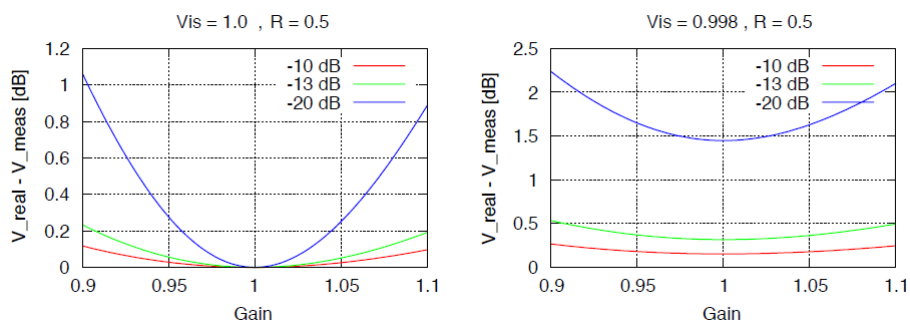


**Figure 5.2.** Electronic gain dependence of the squeezing detection efficiency. Taking the reflectivity to be  $R = 0.5$ , depending on the initial squeezing value ( $10dB$ ,  $13dB$  and  $20dB$ ) and varying the electronic gain, the measured squeezing ( $V_{meas}$ ) diminishes with respect to the real one ( $V_{real}$ ). The situation is even worse if we allow a non perfect fringe visibility (shown in the right panel).

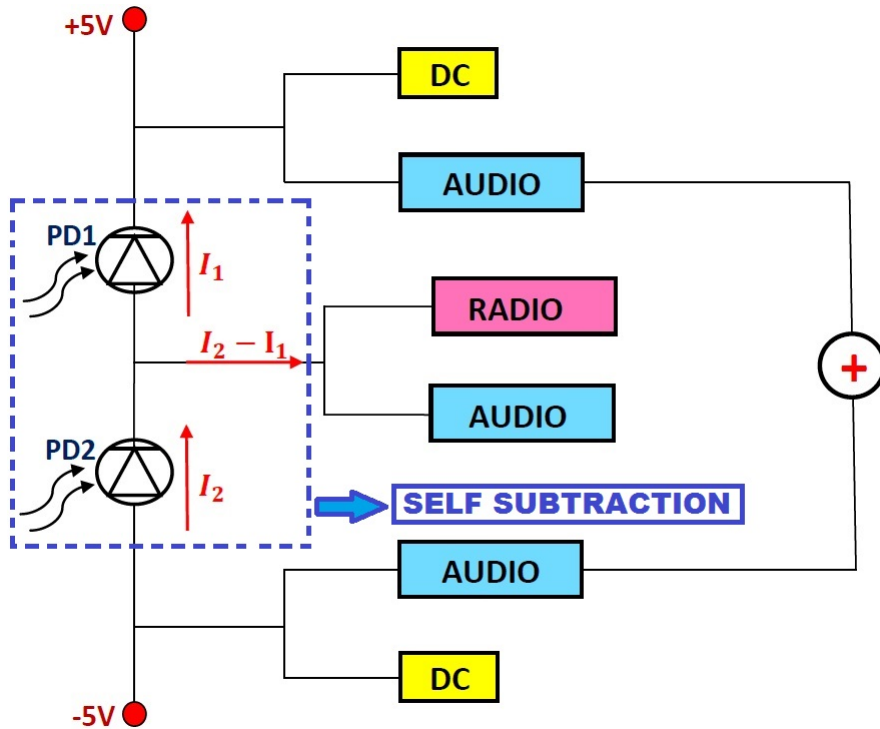


**Figure 5.3.** Conceptual scheme of the circuit design: two photodiodes are kept in reverse bias by a 5V supply and the power of the light impinging on them is detected through the DC blocks. The difference photocurrent is obtained through a self-subtraction scheme and then readout at two different frequency bands: in the Virgo band, i.e. 10Hz-10kHz (AUDIO block); 1MHz-120MHz (RADIO block). The two photocurrents are also detected and summed in the Virgo band. The blocks indicated with DC, AUDIO and RADIO are transimpedance amplifiers for the photocurrents of each photodiode and/or for the difference photocurrent, working at the appropriate frequency band.

- the circuit is designed in order to perform *the sum and the difference between the two photocurrents*: the first output is useful for the diagnostic (as well as the DC output from the single photodiode) and contains the information on the local oscillator shot noise; the second one contains the information on the detected squeezing.
- A *self-subtraction scheme* is adopted in order to reduce the degradation of the squeezing detection due to the electronics. Indeed, any unavoidable electronic unbalance between the electronics connected to the photodiodes would be drastically amplified degrading or completely destroying the measured squeezing value. In the proposed scheme the difference is performed before any amplification, taking the signal from a node between the two photodiodes, so that the two photocurrents are added with opposite signs; then the resulting current is amplified by a dedicated block.
- The bias of the two photodiodes is performed by using a *unique power supply reference* (a typical value is 5 V), from which also the negative power supply is derived. In this way, fluctuations in the power supply appear as a common-mode effect for both photodiodes.

### Low noise design requirement

The power spectrum of the sum photocurrent should correspond to the shot noise power spectrum of the local oscillator. The power spectrum of the difference photocurrent, which contains the quantum fluctuations of the squeezed field, can be below or above the shot noise level of the local oscillator depending on which quadrature we are measuring, and equals the shot noise level

for an unsqueezed vacuum.

Assuming, for example, a squeezing level of  $11dB$ , i.e a factor  $e^{-2r} \sim 3 - 4$ , we require that the total circuit noise at the readout block outputs of the sum and the difference photocurrents have to be at least ten time below the output signals due to the shot noise.

## Frequency response

As shown in fig. 5.3, the circuit prototype is designed in order to have the following outputs:

- *DC readout for each photodiodes*

It is needed to check if both the photodiodes receive the same amount of light.

- *AUDIO-BAND AC readout 10 Hz – 10 kHz*

It is performed for the photocurrent of each photodiode and for the difference photocurrent at sideband frequencies in Virgo band  $10\text{ Hz} - 10\text{ kHz}$  around the local oscillator carrier frequency. The sum of the two photodiodes' photocurrents is also performed.

- *RADIO-BAND AC readout 1MHz – 120 MHz*

Since it is difficult to balance the circuit on this large electronic bandwidth and since the sum of the two photocurrents is useless for the characterization of squeezing, the idea is to suppress this element at the radio band, thus in this block there is only readout of the photocurrent difference.

## Circuit design

The circuit is designed with the help of appropriate simulation tools, as the *Spice* simulation, performed with both *Cadence* and *Tina*. Subsequently a theoretical noise estimation is obtained with the aid of a dedicated code developed with *MatLab* (see sec. 5.1.4).

The detailed electronics schematics of the detection board are reported in the following figures 5.4, 5.5 and 5.6.

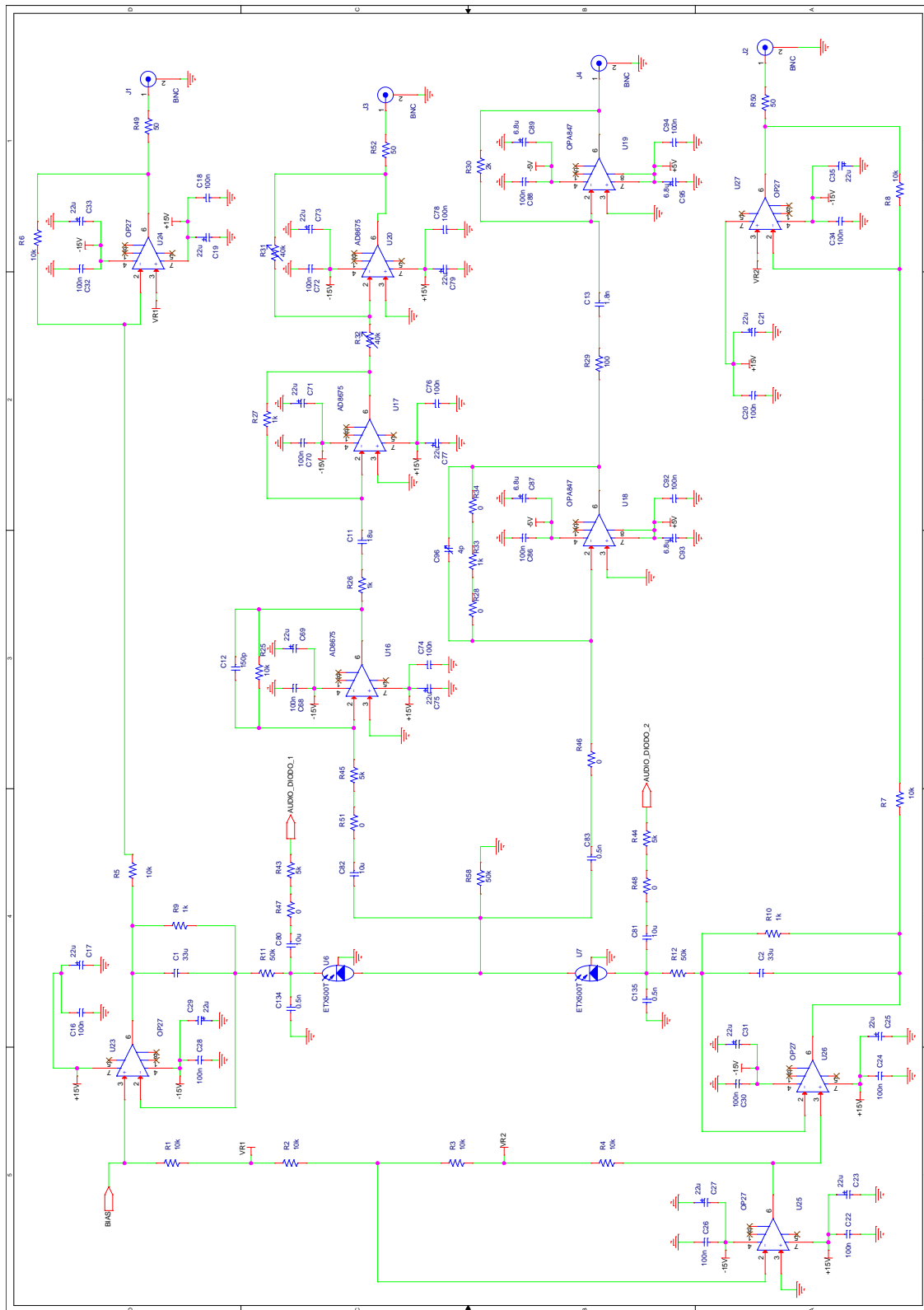
**!!!!ATTENTION: THE FOLLOWING SCHEMES MUST BE UPDATED WITH THE NEW ONES (redesigned board) !!!!**

### 5.1.2 The photodiode selection

In the previous section we have outlined the design of a low noise circuit able to measure fluctuations below the shot noise level of the local oscillator. In order to keep the low noise requirement, diodes with low dark current are desirable. In addition, the local oscillator should be as intense as possible in order to better enhance the detection of the squeezed field (and, of course, the detection of the local oscillator shot noise itself). Thus, photodiodes able to bare much intense light beams are useful too. These two requirements can be in contrast, so that a trade off between these two characteristics are needed.

We focused our attention on two photodiodes, the EPITAXX ETX500T and the HAMAMATSU G7096. Their most useful characteristics in terms of the circuit design are reported in Tab. 5.1.

As shown in the table, the EPITAXX photodiodes have a much lower dark current ( $12\text{ nA}$  vs  $5\text{ }\mu\text{A}$ ) with respect to the HAMAMATSU and can bare an higher maximum optical power ( $10-11\text{ mW}$  vs  $2\text{ mW}$ ). Those characteristics make the EPITAXX photodiodes more convenient



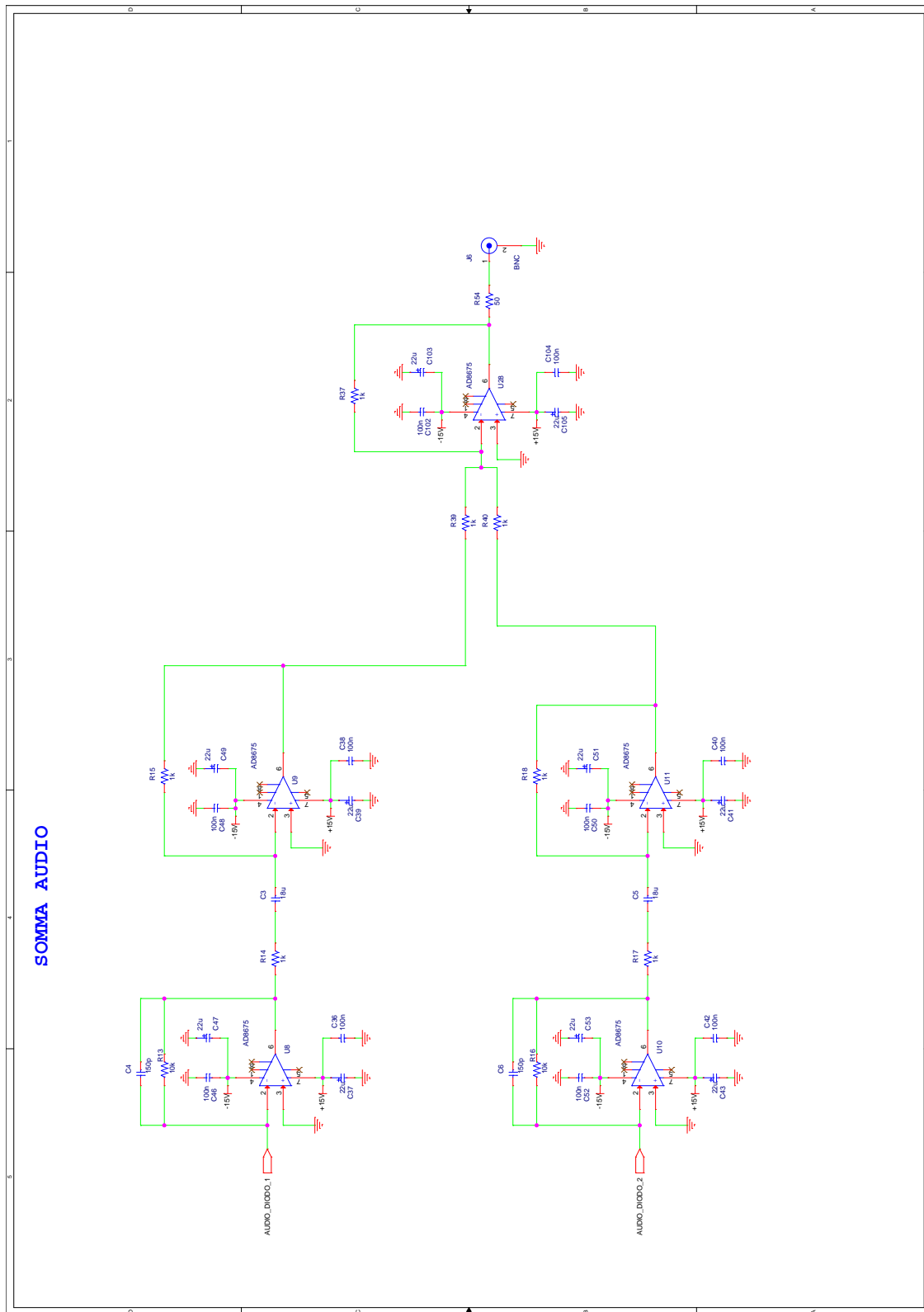


Figure 5.5. Scheme of the circuit prototype: page 2

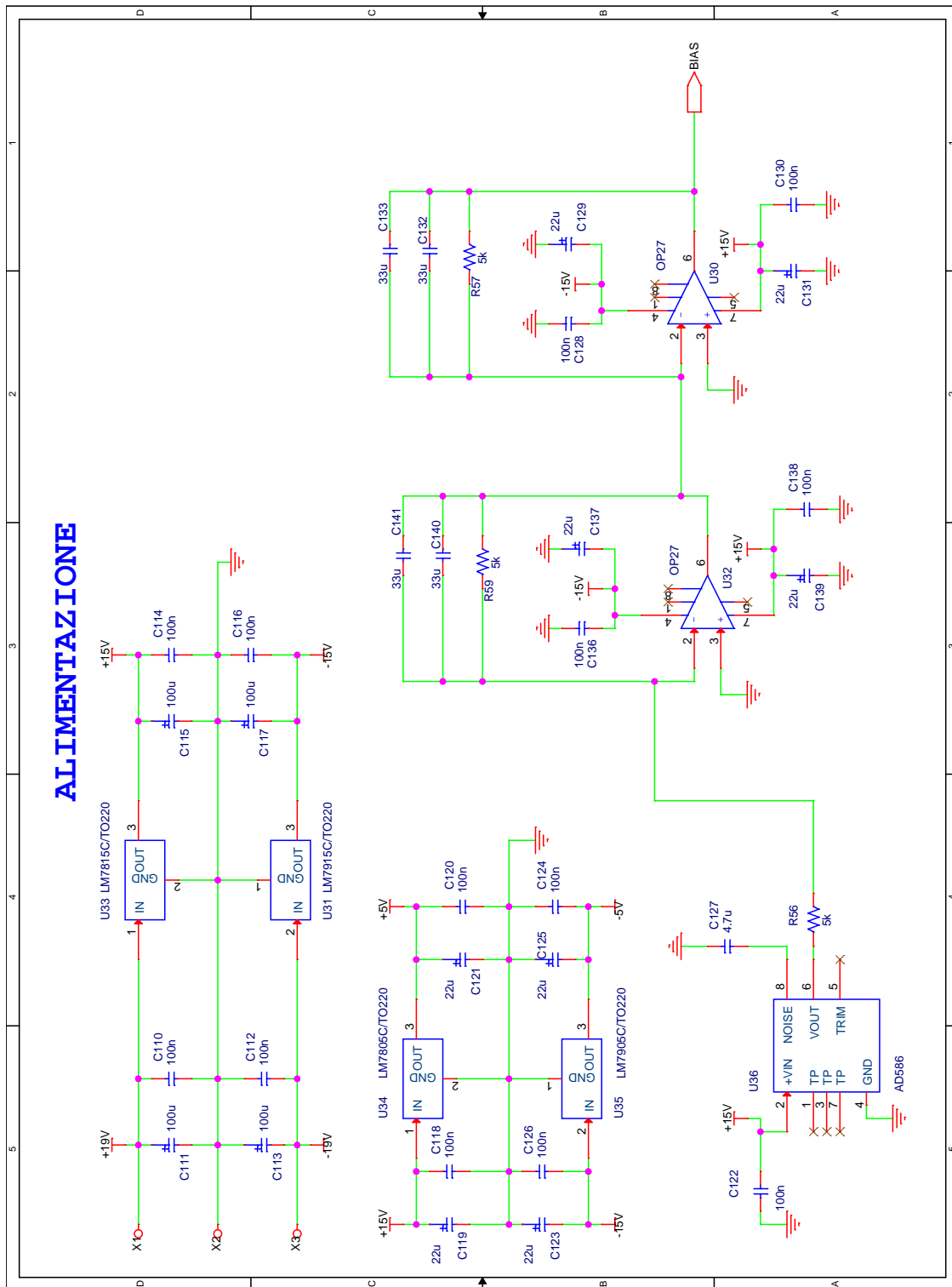
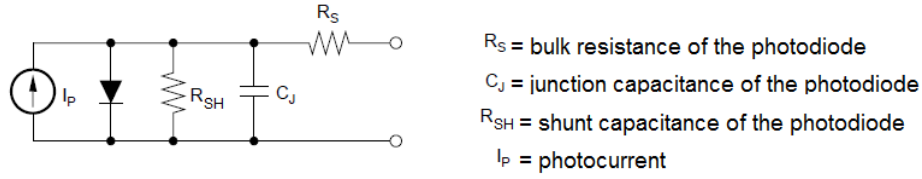


Figure 5.6. Scheme of the circuit prototype: page 3

	EPITAXX ETX550T	HAMAMATSU G7096
DARK CURRENT	12 nA	5 $\mu$ A
TIME RISE/FALL	2.5 ns	60 ps
AREA	500 $\mu$ m <sup>2</sup>	200 $\mu$ m <sup>2</sup>
MAX POWER	10 – 11 mW	2 mW
SHUNT RESISTANCE	250 M $\Omega$	n.a.
JUNCTION CAPACITANCE	15 pF	n.a.
BULK RESISTANCE	25 $\Omega$	n.a.

**Table 5.1.** Characteristics of the photodiode models EPITAXX ETX500T and HAMAMATSU G7096 necessary for the detection board.



**Figure 5.7.** Equivalent circuit of a photodiode.

than the HAMAMATSU. Moreover, the EPITAXX photodiodes have a larger sensitive area than the HAMAMATSU (500  $\mu$ m<sup>2</sup> vs 200  $\mu$ m<sup>2</sup>), a characteristic which is obviously advantageous for a practical implementation. On the other hand, the larger is the area, the slower is the response of the photodiode and the narrower is the available detection bandwidth. In particular the EPITAXX photodiodes have a much higher rise/fall time than the HAMAMATSU (2.5 ns vs 60 ps) and the detection band that they can cover is at most of  $\sim 150$  MHz, while the HAMAMATSU can cover several hundreds of MHz.

The photodiodes are schematized by the equivalent circuit shown in fig. 5.7. The generator is the photocurrent source, while  $R_{SH}$  and  $C_J$  are the resistor and the capacitor of the semiconductor junction and  $R_S$  the bulk resistance of the photodiode in series to all these other electric elements. The bias circuit of the photodiodes has to be realized starting from a high precision 5 V DC supply. This supply is obtained by filtering, through a double stage low pass filter (cut-off frequency at 0.5 Hz), the +5 V supply exiting from the high-precision +5 V reference device AD586 (see fig. 5.6). The -5 V supply is obtained from the +5 V reference through the circuit shown in fig. 5.8. Using the properties of ideal op-amps, we have that the current  $i$  is given by:

$$i = \frac{V_A - V_C}{2R} = \frac{V_C - V_B}{2R} = \frac{V_{BIAS}}{2R} = -\frac{V_B}{2R} \quad (5.1)$$

Thus we easily obtain that:

$$V_B = -V_{BIAS} \quad V_{R1} = \frac{V_{BIAS}}{2} \quad V_{R2} = -\frac{V_{BIAS}}{2} \quad (5.2)$$

In this way, the photodiodes are kept in reverse bias by the two supplies at  $\pm V_{BIAS}$  ( $\pm 5$  V), as shown in fig. 5.8. The advantage of this set-up is that the -5V supply comes from the 5 V supply, thus every fluctuation of the 5V supply reflects in an equal fluctuation of the -5 V supply. This greatly help from a point of view of the electronic balance, a characteristic of the circuit which, as we stressed, is extremely important when detecting squeezed light.



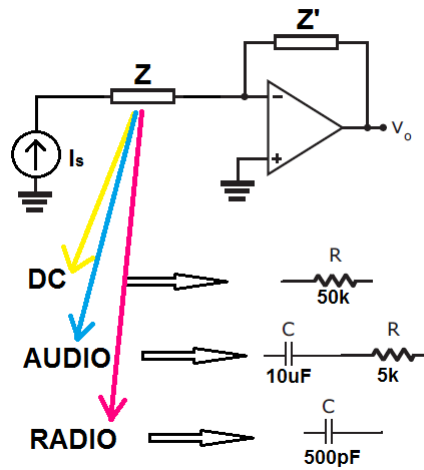


**Figure 5.9.** Input impedances, in case of ideal operational amplifier for the DC, AUDIO and RADIO blocks.

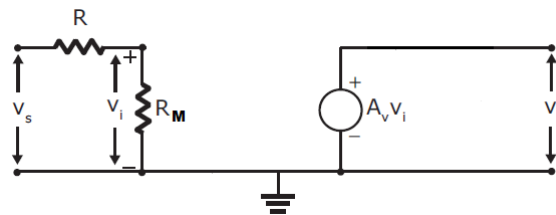


**Figure 5.10.** From the signal  $v_s$  point of view, the op-amp with feedback impedance  $R'$  can be seen as a device with input impedance  $R_M$  (it comes out from the Miller theorem) which amplify by  $A_v$  the difference of the voltages at its two input ports.

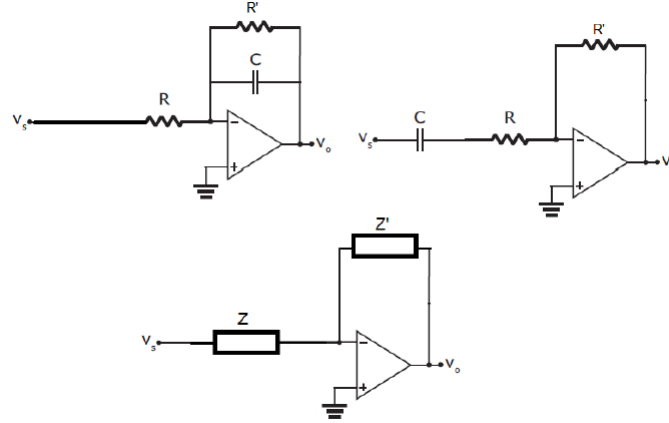


**Figure 5.11.** *upper-left panel:* inverting low-pass filter. *upper-right panel:* general inverting filter. *lower panel:* inverting high-pass filter.

shunt resistance and the junction capacitance. Referring to fig. 5.9 and fig. 5.10, we have:

$$Z_M = \frac{Z'}{1 - A_v} \tag{5.3}$$

where  $Z'$  is the feedback impedance of the transimpedance amplifier and  $A_v$  is the open-loop gain of the operational amplifier.

The choice of the feedback impedances and the characteristics of the operational amplifiers chosen for the various blocks will be discussed later when we will analyze in more details the design of each block. Here we summarize just few basic information, on the base of which we compute the Miller contribution to the input impedances.

We assume that for all the selected operational amplifier the open-loop gain is described by a function of the form:

$$A_v = \frac{A_0}{1 + i \frac{\nu}{\nu_{co}}} \tag{5.4}$$

while the feedback impedance is that of the low-pass filter shown in fig. 5.11. Indicating by  $R_F$  and  $C_F$  the feedback resistance and capacitance respectively, in order to clarify the design strategy and illustrate by quantitative plots, we assume typical values of commercial amplifiers<sup>2</sup>:

- *DC*  
 $R_F = 1k\Omega$       $C_F = 33\mu F$       $A_0 = 1.8 \times 10^6$       $\nu_{co} = 40Hz$
- *AUDIO*  
 $R_F = 10k\Omega$       $C_F = 150pF$       $A_0 = 10^6$       $\nu_{co} = 10Hz$
- *RADIO*  
 $R_F = 1k\Omega$       $C_F = 4pF$       $A_0 = 8 \times 10^4$       $\nu_{co} = 5 \times 10^4 Hz$

Let us note that, as shown in fig. 5.12, in the three interesting frequency bands, DC, 10 Hz – 10 kHz for AUDIO and 1MHz – 100 MHz for RADIO, the impedance of the corresponding detection block is well below the impedances of the other detection blocks and of the photodiode, thus, a signal at a given frequency, in one of the three detection bands, will contribute just to the detection block dedicated for the corresponding detection frequency band.

In addition, the photocurrent due to one photodiode does not leak in the circuitry devoted to the

<sup>2</sup>These values are derived from the specification of the operational amplifiers OP27 for the DC block, the AD8675 for the AUDIO and the OPA847 for the RADIO one.

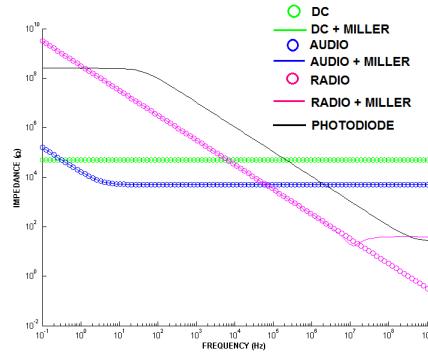


**Figure 5.12.** Plot of the magnitude of the input impedances of the DC, AUDIO and RADIO blocks, both considering ideal operational amplifiers or taking into account the Miller effect. Also the impedance which a photodiode sees toward the other photodiode is plotted.

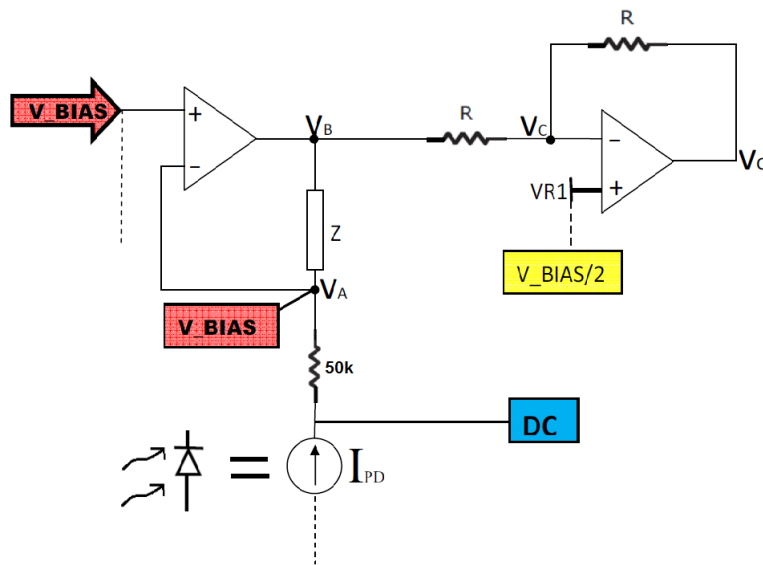


**Figure 5.13.** DC readout block.

other one the other one seen practically as an open circuit, so we can conclude that the amplified signals of the two photodiodes are independent in the frequency band we are considering.

The figure 5.12 shows also that at up to  $\sim 100$  MHz, given the characteristics of the selected operational amplifier and of the transimpedance blocks, the effect of the Miller impedances is negligible. Thus, for our purposes they are considered as ideal.

### The DC readout

The scheme of the DC readout block of the top photodiode of fig. 5.8 is shown in fig. 5.13: the DC part of the photocurrent coming from the photodiode only circulate in the  $50k\Omega$  resistor (which roughly is the input impedance of the DC block) and in the transimpedance indicated with  $Z$ . The point A is at voltage  $V_{BIAS}$ , while the point indicated with  $VR1$  is connected with the point  $VR1$  shown in fig. 5.8 and is at voltage  $V_{BIAS}/2$ . The same description applies to the bottom photodiode of fig. 5.8 but in this case the sign of all voltages is reversed.

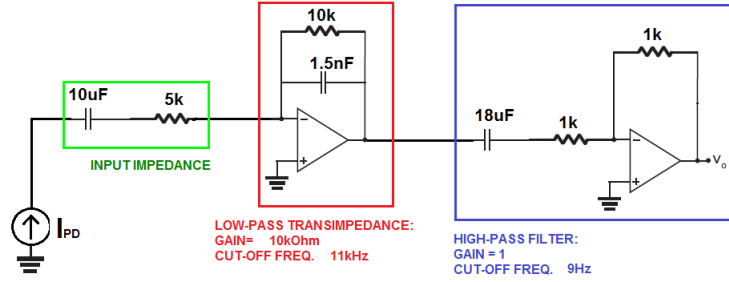


Figure 5.14. AUDIO readout blocks: first and second stage.

We have:

$$V_B = V_A + I_{PD}Z \tag{5.5}$$

$$V_A = V_{BIAS} \tag{5.6}$$

$$i = \frac{V_B - V_{BIAS}/2}{R} = \frac{V_{BIAS}/2 - V_o}{R} \tag{5.7}$$

thus

$$V_o = -I_{PD}Z \tag{5.8}$$

The op-amp with feedback impedance  $Z$  acts as a transimpedance amplifier, while the second stage eliminates from the output voltage the offset, due to the bias voltage, which can be found in the expression for  $V_B$ .

In fig. 5.13 the elements composing  $Z$  are shown: a  $1\text{ k}\Omega$  resistor in parallel to a  $33\ \mu\text{F}$  capacitor, so that the first stage acts as a low-pass transimpedance amplifier with cut-off frequency at  $\sim 5\text{ Hz}$  and transimpedance gain  $1\text{ k}\Omega$ .

### The AUDIO readout (10 Hz – 10 kHz)

The AUDIO blocks for the readouts of both the sum and the difference of the photocurrents, are composed by a low-pass transimpedance as first stage and a high-pass filter as second one, as shown in fig. 5.14<sup>3</sup>.

The first stage has transimpedance gain  $10\text{ k}\Omega$  and low-pass cut-off frequency  $\sim 11\text{ kHz}$ . The second stage has unity gain and high-pass cut-off frequency  $\sim 9\text{ Hz}$ .

The signals exiting the second stage of AUDIO-readout blocks of the two photodiode photocurrents, are then summed with a unity gain circuit as that shown in fig. 5.15.

Then, a third stage is added to the readout block of the photocurrent difference. This stage, shown in fig. 5.15 is only a unity gain stage, which is needed to balance for noise measurement porpoise the sum and difference circuit blocks.

### The RADIO readout (1 MHz -100 MHz)

The design of the RADIO block requires more care than that of the other blocks. This is due to several reasons:

- The photodiodes have a junction capacitance of the order of  $10 - 15\text{ pF}$  and, in the selected frequency band, it can severely affect the frequency response of the amplifier.

<sup>3</sup>We assume that all the AUDIO stages make use of the op-amp model AD8675.

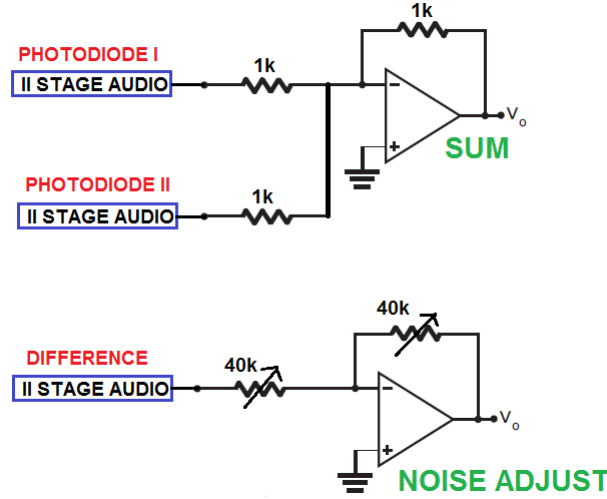


**Figure 5.15.** AUDIO readout blocks. *Top:* sum stage of the single-photodiodes readout blocks. *Bottom:* third stage of the difference photocurrent readout block.

- The op-amps, which can cover the bandwidth  $1\text{ MHz} - 100\text{ MHz}$  are not stable for unitary values of the voltage gain. This implies to set the gain higher than a given value (usually  $\gtrsim 10$ ), constraining the ratio of the feedback resistance to the input resistance. Moreover, other parasitic elements are unavoidable distributed in the circuitry and if their values is too high, together with the parasitic capacitances, they would act as low pass filter. Usually resistors have a parasitic capacitance of order  $0.5 - 1\text{ pF}$ , and if for example we deal with a  $2\text{ k}\Omega$  feedback resistor in the designed amplifier, its parasitic capacitance determine a low-pass cut-off frequency of order  $\sim 150\text{ MHz}$ . On the other hand, the resistance values should not be too low because op-amps can only drive currents up to a maximum value. The lower-limit is obtained by imposing that supply voltage of the op-amp divided by the resistance is lower than the maximum current, which the op-amp can drive.
- Unlike for the AUDIO readout, it results practically impossible to design a sum and a difference readout RADIO blocks characterized by the same transfer characteristics and the same noise performance. In fact, the addition of an extra stage can change the transfer function of the block. For this reason we choose to install just the RADIO block for the photocurrent difference, which is sufficient for the characterization of of the squeezing level.

The difference photocurrent readout RADIO block is composed of two stages, the first one is a low-pass transimpedance amplifier and the second one a high-pass filter, as shown in fig. 5.16<sup>4</sup>.

If  $R_F$  and  $C_F$  are the feedback resistance and capacitance of the amplifier,  $C_J$  is the junction capacitance of the photodiode,  $C_{OPA}$  is the total input capacitance of the op-amp and  $GBP$  its gain-bandwidth product, a flat response up to a cut-off frequency

$$\nu_{co} = \sqrt{\frac{GBP}{2\pi R_F (C_J + C_{OPA})}} \quad (5.9)$$

<sup>4</sup>The op-amp model used for those stages is OPA847, which is stable for voltage gain  $G > 12$ , has a large gain-bandwidth product  $GBP = 3.9\text{ GHz}$  and a total input capacitance of  $C_{OPA} = 3.7\text{ pF}$ . The datasheet of OPA847 also includes useful advices for the use of the op-amp in some applications. In particular, it provides a way to design a low-pass transimpedance amplifier for photodiodes, which takes into account the junction capacitance of the photodiode and the total input capacitance of OPA847 and guarantees a flat response up to a cut-off frequency, which can be determined once the feedback impedance has been chosen.

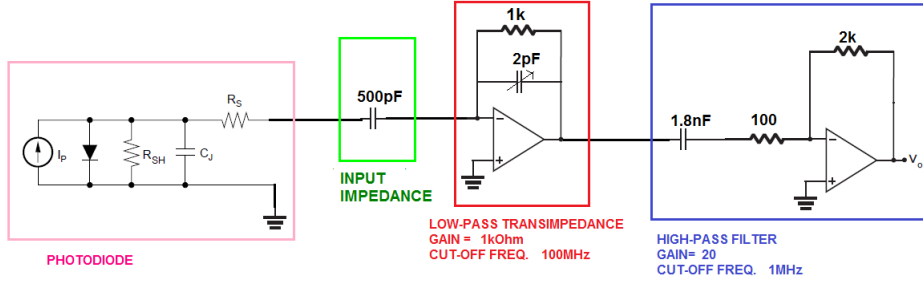


Figure 5.16. RADIO readout blocks: first and second stage.

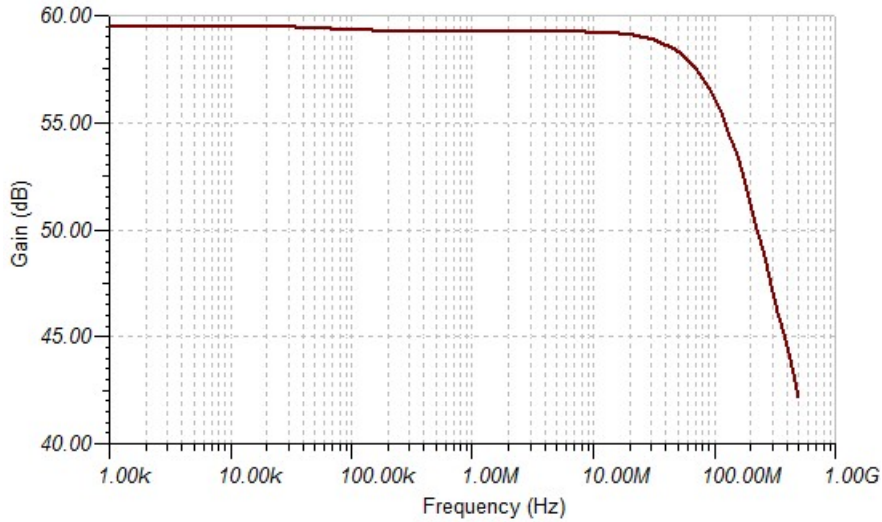


Figure 5.17. RADIO: transimpedance amplifier transfer function.

is achieved when the relation

$$\frac{1}{2\pi R_F C_F} = \sqrt{\frac{GBP}{4\pi R_F (C_J + C_{OPA})}} \quad (5.10)$$

is satisfied. Using the numerical values of the op-amp cited in the footnote, we obtain a transimpedance gain of  $\sim 1\text{ k}\Omega$  and a cut-off frequency of  $\sim 180\text{ MHz}$ . However, in practice this value is expected to be lower when we take into account the contribution of the other photodiode.

The transimpedance transfer function was simulated using the simulation code *Tina*, including both photodiodes: the result is shown in fig. 5.17. The second stage was designed as a high-pass filter with gain 20 and cut-off frequency  $\sim 1\text{ MHz}$  and it is shown in fig. 5.16.

### 5.1.4 Noise budget

In this section we report on the noise study and the performance of the proposed homodyne detector. In the previous section we have set the requirement that the homodyne detector must be able to detect noise levels ten times below the shot noise level of the local-oscillator at least. The shot noise level depends on the local oscillator power and the maximum shot noise level reachable depends on the maximum power that the photodiode can bare. Let us assume that we use as reference value of the order of  $10\text{ mW}$ ).

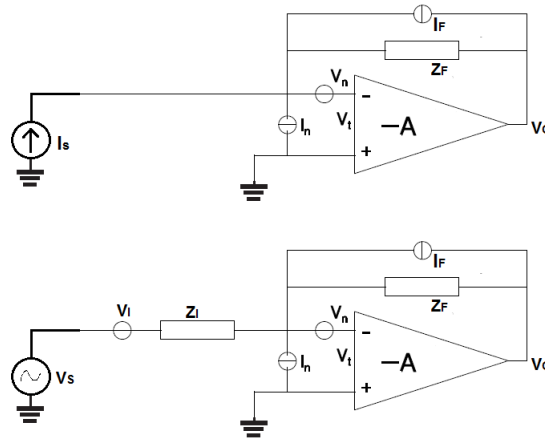


**Figure 5.18.** Schemes used for the noise calculations: on the top the transimpedance amplifier, on the bottom the voltage one.

### Theoretical estimation

The design of the homodyne electronics permits us to assume that the signals of each photodiode, characterized by its power spectrum, is affecting independently the readout blocks of each photodiode.

The photodiode intrinsic noise is due to the thermal noise of the shunt resistance and of the bulk resistance.

The detection blocks contribute also to the total noise, which limits the sensitivity of the measurement of the squeezing factor <sup>5</sup>.

These readout blocks have a first low-pass transimpedance stage and a second high-pass stage, so that the noise calculations refer to the amplifier schemes shown in Eq. 5.18.

In the case of a non-ideal operational amplifier, for an infinite value of the open-loop gain, we obtain:

- *for the transimpedance amplifier:*  
a contributions to the output noise power spectrum (see fig. 5.18);

$$S_{v_n}^{out} = \left| \frac{A}{1+A} \right|^2 v_n^2$$

$$S_{i_n}^{out} = \left| \frac{AZ_F}{1+A} \right|^2 i_n^2$$

$$S_{v_n}^{out} = \left| \frac{AR_F}{1+A} \right|^2 i_F^2$$

- *for the voltage amplifier:*  
here the signal voltage source is short-circuited (see fig. 5.18);

<sup>5</sup>This discussion does not apply to the DC readout of the photocurrents because in this case we are not dealing with noise measurements but with the detection of photocurrents of order of  $mA$  and with output voltages of order of Volts, thus the electronic noise is not a limiting factor.

**v<sub>I</sub>)**

$$\frac{v_I - v_t}{Z_I} = -\frac{v_o - v_t}{Z_F} \quad v_o = -Av_t \quad (5.11)$$

$$v_o = -v_I \frac{Z_F A}{(1+A)Z_I + Z_F} \quad (5.12)$$

thus

$$S_{v_I}^{out} = \left| -\frac{Z_F A}{(1+A)Z_I + Z_F} \right|^2 v_I^2 \quad (5.13)$$

**i<sub>n</sub>)**

$$i_n = \frac{v_t}{Z_I} + \frac{v_t - v_o}{Z_F} \quad v_o = -Av_t \quad (5.14)$$

$$v_o = -i_n \frac{Z_F Z_I A}{(1+A)Z_I + Z_F} \quad (5.15)$$

thus

$$S_{i_n}^{out} = \left| -\frac{Z_F Z_I A}{(1+A)Z_I + Z_F} \right|^2 i_n^2 \quad (5.16)$$

**v<sub>n</sub>)**

$$\frac{v_n + v_t}{Z_I} = \frac{v_o - (v_n + v_t)}{Z_F} \quad v_o = -Av_t \quad (5.17)$$

$$v_o = v_n \frac{A(Z_I + Z_F)}{(1+A)Z_I + Z_F} \quad (5.18)$$

thus

$$S_{v_n}^{out} = \left| \frac{A(Z_I + Z_F)}{(1+A)Z_I + Z_F} \right|^2 v_n^2 \quad (5.19)$$

**i<sub>F</sub>)**

$$v_o - v_t = i_F Z_F \quad v_o = -Av_t \quad (5.20)$$

$$v_o = i_F \frac{AZ_F}{1+A} \quad (5.21)$$

thus

$$S_{i_F}^{out} = \left| \frac{AZ_F}{1+A} \right|^2 i_F^2 \quad (5.22)$$

We developed a MatLab code to simulate the total output noise for both the AUDIO and RADIO difference photocurrent readout blocks and for the AUDIO sum photocurrent readout block. The noise sources of the photodiodes as well as those of the other blocks have been taken into account <sup>6</sup>. For example, the 50 kΩ input impedance of the DC blocks contributes with its

<sup>6</sup>The noise model for the homodyne detector design presented here, is based on the assumption that the contribution comes from the resistance Johnson noise. The 1/f noise contribution is not included because it seems to be negligible on the base of the informations reported in the data sheets of the op-amp that we have considered.

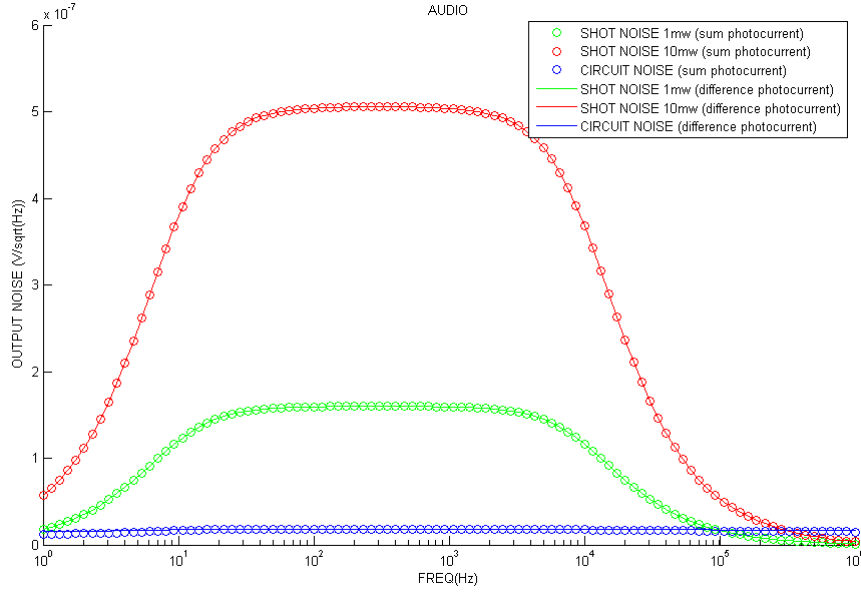


**Figure 5.19.** Noise simulation for AUDIO sum and difference photocurrents' readout blocks.

thermal noise to the output noise of the nearby AUDIO block. Such a kind of contributions can be easily taken into account by appropriately defining the generic impedance  $Z_I$ , which appears in fig. 5.18.

The circuit noise at the output of the AUDIO sum and readout blocks of the photocurrent difference has been plotted in fig. 5.19, together with the shot noise level at the same outputs (which represent the signal), simulated for laser powers 1 mW and 10 mW.

The same has been done in fig. 5.20 for the RADIO difference photocurrents' readout block. In both figures we note that the shot noise level associated to a laser power of 10mW is at least ten times above the intrinsic noise level of the circuit. In addition, the noise and the signal for the AUDIO sum and difference appear to be more or less equal, as required for the electronic balance of the homodyne detector. This result is achieved by adding the third unity-gain extra stage to the difference photocurrent readout block, as shown in fig. 5.15. In fact, this stage compensates the extra noise coming from the summing amplifier and from the fact that, while the difference is performed with the self subtraction scheme and then amplified, the sum is performed after that the two photocurrents have been amplified, and thus at the output of the sum block there is an extra noise contribution in addition to the respect of what happens at the output of the difference block.

## Electronic noise measurement

Following the design presented above we realized a first prototype of the homodyne detection electronic board, mounting on it two *Epitaxx ETX500T* photodiodes, as shown in fig. 5.21. In order to measure the effective electronic noise at the output of the AUDIO difference circuit<sup>7</sup>, the two photodiodes were darkened. The impedance at this output is  $Z_{A-} = 0.04 \Omega$  and the measured voltage noise is plotted in fig. 5.22 and 5.23 for two different frequency bands (1 Hz - 100 Hz and 100 Hz - 10 kHz).

<sup>7</sup>As stated above, the information about the squeezing factor is contained into the AUDIO difference signal, so an electronic low-noise background at this output is crucial.

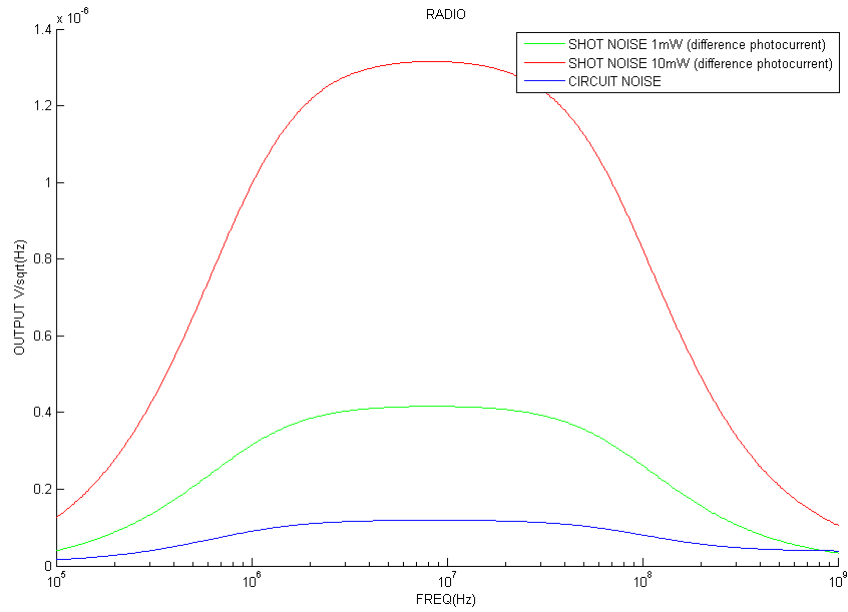


**Figure 5.20.** Noise simulation for RADIO difference photocurrent readout block.



**Figure 5.21.** The first prototype of the homodyne detector electronic board. Two *ETX500T* photodiodes are fixed to the two small holes at the right side of the box, while on the other side there are standard *lemo* connectors for the various read-out blocks (DC 1 and 2, AUDIO sum and difference, RADIO difference, see sec. 5.1.3).

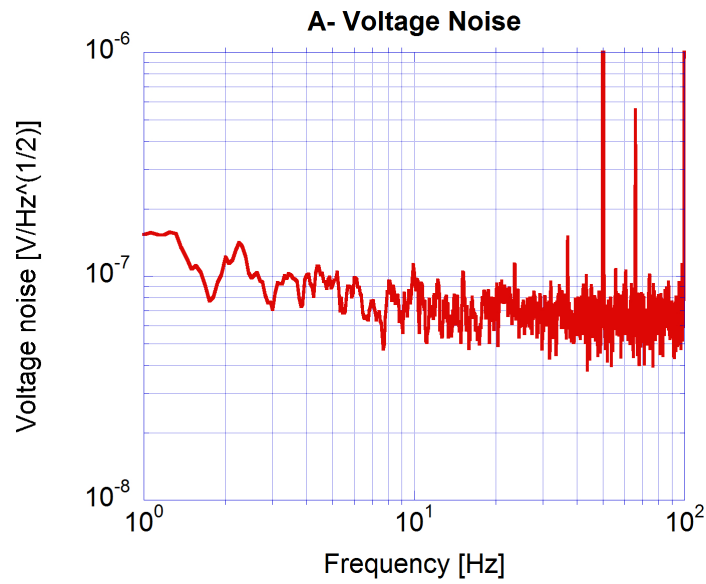


**Figure 5.22.** Voltage noise measured at the output of the AUDIO difference circuit in the frequency band 1 Hz - 100 Hz.

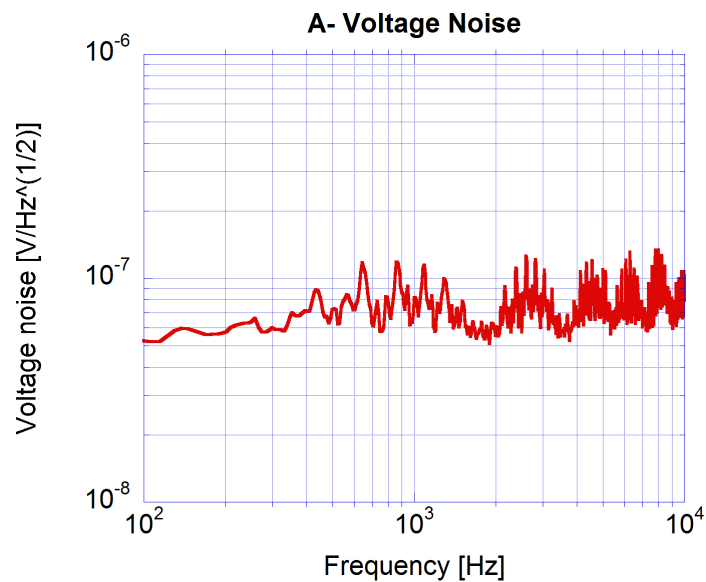


**Figure 5.23.** Voltage noise measured at the output of the AUDIO difference circuit in the frequency band 100 Hz - 10 kHz.

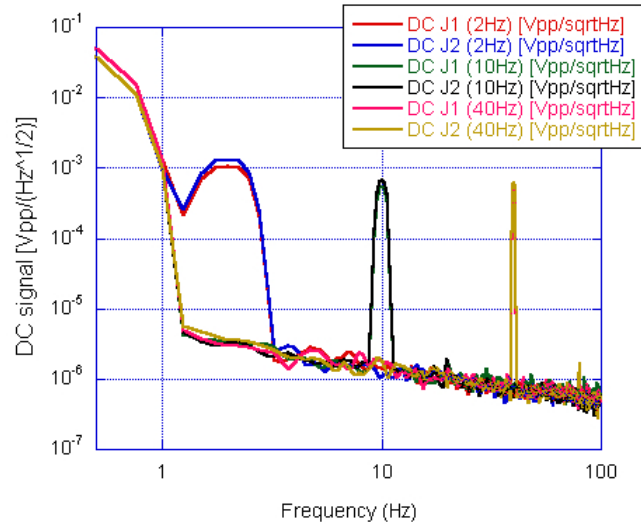


**Figure 5.24.** Response of the DC readout blocks (DC J1 and DC J2) at various offset and pulsating signals emitted by IR LEDs in the frequency band 1 Hz - 100 Hz.

### DC readout response

The response of the DC readout blocks of the first prototype of the detection board was tested by using IR emitting LED placed in front of the two *Epitaxx ETX500T* photodiodes and powered through a standard function generator in order to generate offset and pulsating signals. The DC readout proved to work properly, detecting the input signals at the several frequencies at which it was tested, as shown for example in fig. 5.24 and 5.25.

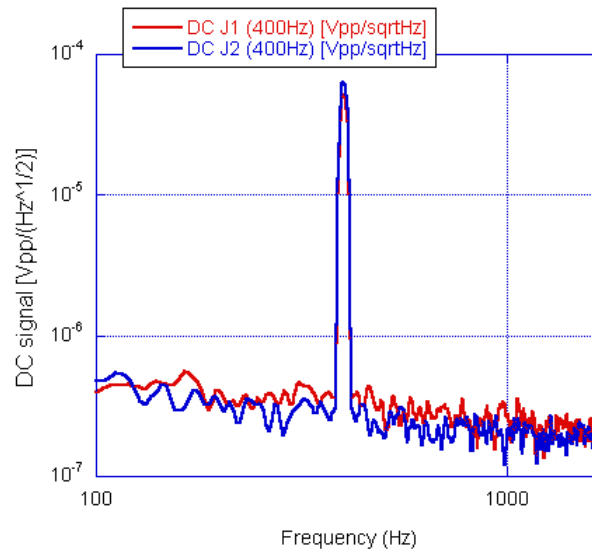


**Figure 5.25.** Response of the DC readout blocks (DC J1 and DC J2) at various offset and pulsating signals emitted by IR LEDs in the frequency band  $100 \text{ Hz} - 2 \text{ kHz}$ .